Journal of Power Sources 195 (2010) 4065–4071

Contents lists available at ScienceDirect

Journal of Power Sources

journal homepage: www.elsevier.com/locate/jpowsour

Sulfated zirconia as a proton conductor for fuel cells: Stability to hydrolysis and influence on catalysts

Satoshi Tominaka [a], Toshiyuki Momma [a], Bruno Scrosati [b], Tetsuya Osaka [a,*]

[a] Department of Applied Chemistry, Graduate School of Advanced Science and Engineering, Waseda University, Okubo 3-4-1, Shinjuku, Tokyo 169-8555, Japan
[b] Department of Chemistry, University of Rome "La Sapienza", P. le Aldo Moro, 5, 00185 Rome, Italy

ARTICLE INFO

Article history:
Received 9 November 2009
Received in revised form 12 January 2010
Accepted 22 January 2010
Available online 1 February 2010

Keywords:
Sulfated zirconia
Fuel cell
Proton conductor
Electrolyte
Catalytic activity

ABSTRACT

Sulfated zirconia is an inorganic solid superacid having sulfate groups covalently bonded to its surface. In this work, sulfated zirconia is synthesized by a solvent-free method to obtain it in the nanoparticle form. This nanostructured sulfated zirconia has been evaluated in terms of (i) chemical stability to hydrolysis and to hydrogen peroxide by thermogravimetric analysis, and (ii) influences on Pt catalyst activity by cyclic voltammetry using sulfated-zirconia dispersion as a supporting electrolyte solution. The results demonstrate that our sulfated zirconia is stable almost perfectly to hydrolysis but partly decomposed by a Fenton reagent containing hydrogen peroxide and Fe^{2+}. In addition, we show that oxygen reduction activity of Pt catalyst in a sulfated-zirconia dispersion is comparatively high (specific activity at 0.9 V *vs.* RHE, $i_{0.9}$: *ca.* 17 μA cm^{-2}) compared to that in a 0.5 M sulfuric acid solution ($i_{0.9}$: *ca.* 15 μA cm^{-2}). Finally, we demonstrate that sulfated zirconia does not influence hydrogen oxidation reaction. These results lead us to conclude that sulfated zirconia is a promising proton conductor for fuel cells.

1. Introduction

Advanced proton conductors are the key materials for the successful commercialization of polymer electrolyte fuel cells (PEFCs), since the conventional ones, *i.e.*, Nafion™ (DuPont), or a sulfonated tetrafluoroethylene copolymers, though having high proton conductivity and chemical and electrochemical stability, are considerably expensive. Since PEFCs consist of a proton conducting membrane and two catalytic porous electrodes using precious metal catalysts (generally, Pt nanoparticles), developments of low-cost proton conductor alternatives to the conventional Nafion are of great practical importance. To be suitable for PEFCs, proton conductors must fulfill several requisites, including (i) high conductivity, (ii) high stability, (iii) low influence on catalyst activity and (iv) low cost.

Polymer alternatives to Nafion, including Nafion-based composites [1,2] and hydrocarbon polymers [2,3], have been synthesized, especially for the applications as membranes. Most hydrocarbon polymers seem to be oxidized by Pt catalyst especially on the cathode side due to the high electrode potential. In this respect, inorganic proton conductors, *e.g.*, sulfated oxides (*e.g.*, sulfated zirconia) [4], zeolite [5], phosphotungstic acid [6,7] and hydrated oxides (*e.g.*, titania and zirconia) [8,9], are quite promising alternatives.

In this scenario, our work has been focused on sulfated zirconia as such or as an additive to Nafion for both electrolyte membranes and catalyst layers. Sulfated zirconia is an inorganic solid superacid which consists of zirconia particles having sulfate groups covalently bonded to their surface (Fig. 1). Considering its favorable properties that include: (i) high proton conductivity associated with the surface groups, (ii) high thermal stability (up to ~600 °C), and (iii) easy synthesis procedure, sulfated zirconia has attracted interest as an additive to PEFC electrolyte membranes [10–14]. Such composite membranes exhibit promising performance for low-humidity and medium temperature operation of PEFCs, this being important in terms of reaction kinetics and of reduction of the amount of expensive Pt catalysts. For example, results previously obtained in one of our laboratories showed that a sulfated zirconia-doped Nafion membrane has a high proton conductivity (>10^{-2} S cm^{-1}) in a 60–150 °C temperature range [11]. In addition, our research group synthesized sulfated zirconia nanoparticles and reported that they are highly conductive proton conductors (13 ± 3 mS cm^{-1} at 30 °C, 100%-RH) and electrochemically stable in the potential range of interest for PEFC reactions [15].

Results are promising since they outline the good behaviors of sulfated zirconia as a valid proton conductor for PEFCs. Some concerns, however, still remain on its chemical stability, *e.g.*, to hydrolysis and to oxidation caused by hydrogen peroxide, and on its influence on catalyst. They are key aspects to finally evaluate

* Corresponding author. Tel.: +81 3 5286 3202; fax: +81 3 3205 2074.
E-mail addresses: tominaka@aoni.waseda.jp (S. Tominaka), osakatets@waseda.jp (T. Osaka).

0378-7753/$ – see front matter © 2010 Published by Elsevier B.V.
doi:10.1016/j.jpowsour.2010.01.053

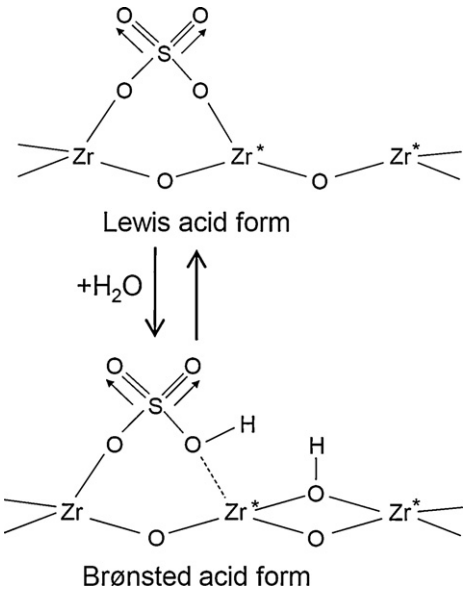

Fig. 1. Scheme of a surface model of sulfated zirconia as proposed by Bolis et al. [31].

the feasibility of sulfated zirconia as proton conductor for PEFCs. Therefore, this work was addressed to their clarification.

2. Experimental

Sulfated zirconia nanoparticles were synthesized by following our previously published method [15]. In brief, zirconium oxychloride and ammonium sulfate were separately ground and then mixed until becoming a sticky paste. The paste was dried under ambient conditions for 18 h and then calcined at 600 °C for 5 h under air flow (400 mL min^{-1}). The particle size was confirmed to be very small, 5–10 nm, by transmission electron microscopy [15]. The particles were further analyzed by X-ray photoelectron spectroscopy (XPS) (JPS-9010TR, JEOL) applying a Mg Kα radiation at 10 kV, 10 mA. The energy scale was calibrated using carbon 1s peak (284.1 eV). The textural properties of the powder were analyzed by nitrogen adsorption–desorption measurement (Belsorp mini, Bel Japan, Inc.).

The chemical stability of the sulfated zirconia nanoparticles was evaluated by determining decreases in sulfate-group content after boiling or their immersion in a hydrogen peroxide solution. The decreases were determined from thermogravimetric analysis (TGA) (SDTA851e, Mettler Toledo, 25–1000 °C, in air). The sulfated zirconia was boiled in pure water (2.74 g L^{-1}) in a oven (150 °C, air) until drying (~8 h), or was treated in a Fenton reagent (1 g L^{-1}), which contained 3 vol% hydrogen peroxide solution and 2 ppm Fe^{2+} ($FeSO_4 \cdot 7H_2O$, Merk), at 80 °C for 3 h. The particles precipitated during the test, then were filtrated using a nitrocellulose membrane filter (0.025 μm, Millipore) and then dried at 50 °C overnight. Since some concerns remained on missing some of nanoparticles through the filter, we also recovered the particles by pouring the solution into an excess amount of ethanol and then dried the precipitate at 50 °C overnight. The TGA results of the both samples were the same, meaning that the particles were accurately collected even by the filtration test.

The influence of sulfated zirconia nanoparticles on the catalytic activity of Pt catalyst was evaluated by controlling the oxygen reduction reaction (ORR) and the hydrogen oxidation reaction (HOR), using a sulfated-zirconia dispersion as a supporting electrolyte solution. The dispersion was prepared by following our previously published method [15]: Basically, sulfated zirconia powder was once dispersed in pure water (2.74 g L^{-1}) and then heated at 150 °C until drying to remove electrochemically reactive impurities [15]. The dried powder was re-dispersed in pure water. To further reduce the amount of impurities, a very low concentration, 2.74 g L^{-1}, *i.e.*, about one-seventh of the dispersion used in our previous work [15], was chosen.

The ORR was evaluated by cyclic voltammetry (CV) in the potential range of 0.4–1.1 V at 10 mV s^{-1}. The HOR was evaluated in the potential range of the open circuit potential to 0.4 V at 10 mV s^{-1}. These electrochemical measurements were conducted at room temperature using a Pt rotating-disc-electrode (BiStat, PAR) at 2000, 1000, 500, 250 and 125 rpm in a three-electrode cell containing the sulfated-zirconia dispersion as supporting electrolyte. The potential was referred to a reversible hydrogen electrode (RHE), which was prepared by evolving hydrogen bubbles on a Pt wire soaked in the supporting electrolyte solution separated from main compartment by a porous glass. A Pt coil was used as the counter electrode.

3. Results and discussion

3.1. Characterization of the sulfated zirconia

To enhance the understanding of the following analyses, we characterize the synthesized sulfated zirconia in detail. We reported that the sulfated zirconia had a small particle size of 5–10 nm, a sulfur content of 9.5 ± 1 wt%, a low crystallinity and a superacidity in a dry state (acidity strength: min −13.16) [15]. The sulfur groups were confirmed to be present even after rinsing with pure water [15]. The atomic ratio of sulfur to zirconium (S/Zr) was *ca.* 0.75 determined by energy dispersive X-ray spectroscopy. Such a considerably high sulfur content probably originates from the presence of sulfate in the bulk phase as reported by Cutrufello et al. [16] and Fărcaşiu et al. [17], or from the presence of polysulfate [18]. In the former case, they reported that the sulfates in the bulk phase decreased the crystallinity of zirconia, and this probably occurred in our sample as indicated by the low crystallinity (Fig. 2).

The surface atomic ratio was determined from the XPS analysis (Fig. 3) to be *ca.* 0.70 (S/Zr). Comparing this value with the bulk ratio, we found the presence of sulfate also in the subsurface phase. Fig. 3 shows that the S 2p peak exhibits a typical feature for sulfated zirconia, *i.e.*, a pronounced asymmetry. Parvulescu et al. [19] decomposed the peak to two components. One was located around 169 eV, which could be assigned to deprotonated sulfated species, and another around 170 eV, which could be assigned to protonated ones. The O 1s was located at 531.9 eV, which is attributed to sulfate, and a shoulder peak was observed around 530 eV, which

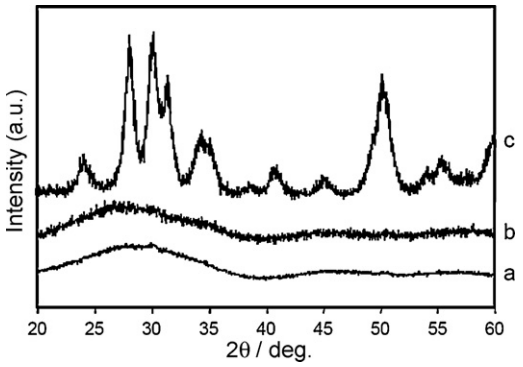

Fig. 2. XRD patterns of the sulfated zirconia synthesized by the solvent-free method: (a) as-synthesized sample, and (b) the boiled sample. For comparison, (c) a typical sulfated zirconia with a mixed crystalline form of the monoclinic phase of zirconia (28.3° and 31.5°) and the tetragonal phase of zirconia (30.2°) is shown [15].

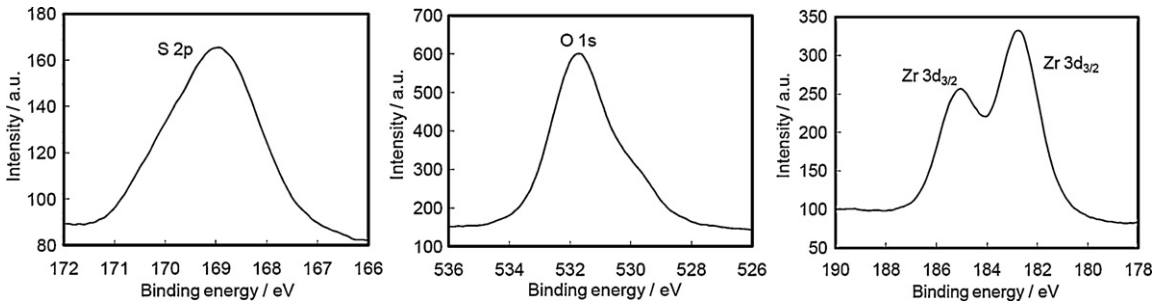

Fig. 3. X-ray photoelectron spectra of the synthesized sulfated zirconia.

is attributed to zirconia [20]. The Zr 3d doublet peaks are located at 182.9 eV for $3d_{5/2}$ and 185.2 eV for $3d_{3/2}$, which are higher than those of ZrO_2 (182.0 eV for $3d_{5/2}$ [20,21]). Since it is known that sulfation shifts the Zr 3d peaks toward higher binding energy, the data and the absence of the ZrO_2 peaks suggest our sample contained sulfate also in the bulk phase.

One may concern that the subsurface sulfate does not contribute to ionic conduction, but the concern will be swept aside by the following consideration. As we reported previously [15], this sulfated zirconia exhibited a high ionic conductivity ($17 \pm 3\,mS\,cm^{-1}$) in a state of dispersion at a concentration of $20.4\,g\,L^{-1}$, which equals to an acid concentration of 61 mM (acid content: $3.0\,mmol\,g^{-1}$). Comparing this value to its proton concentration, 79 mM (pH: 1.1 at 25 °C) [15], we found that some of the protons probably originated from the subsurface sulfate groups, *i.e.*, the subsurface sulfate groups also became the acidic sites as shown in Fig. 1. Probably, the sulfated zirconia absorbed water to dissociate protons also from the subsurface sulfates.

The textural properties of the sulfated zirconia powder were analyzed by nitrogen adsorption–desorption measurements. From the adsorption isotherm (Fig. 4), the specific surface area was determined by the BET method ($35\,m^2\,g^{-1}$), and the mesopore size (radius: 4.5 nm) and the cumulative pore volume ($0.07\,cm^3\,g^{-1}$) were analyzed by the BJH method (see the inset of Fig. 4). Our data are well consistent with those of a sulfated zirconia with a high sulfur content reported by Cutrufello et al. ($31\,m^2\,g^{-1}$, 5.9 nm, $0.08\,cm^3\,g^{-1}$) [16], and they attributed the small surface area to the lack of pore volume in the powder state. The BET surface area was relatively low as sulfated zirconia. Assuming that the acidic sites were only on the surface, the number of the sites is calculated as $51\,nm^{-2}$. This value is too high for monolayer of the sulfate groups [19], thereby supporting our consideration that some of the sulfur groups also exist in the subsurface phase. Thus, we conclude that the synthesized sulfated zirconia nanoparticles had acidic sites also in the subsurface phase.

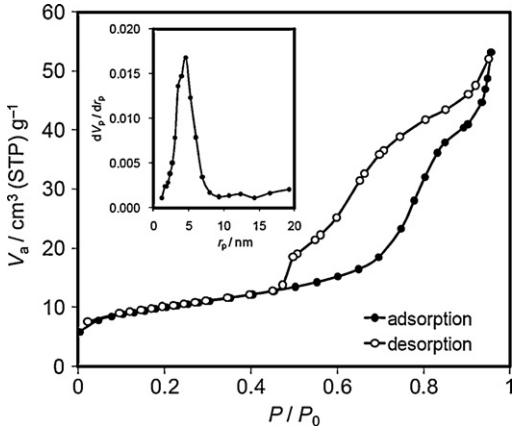

Fig. 4. Nitrogen adsorption–desorption isotherms for the as-synthesized sulfated zirconia powder. The inset shows pore-size distribution curve (the BJH plots from the adsorption isotherm). r_p and V_p mean pore radius (nm) and pore volume ($cm^3\,g^{-1}$), respectively.

3.2. Chemical stability of sulfated zirconia

The chemical stability of the sulfated zirconia nanoparticles was investigated by TGA. Fig. 5 shows the TGA curve for the as-prepared sample exhibiting two weight losses (Fig. 2a): a gradual loss associated with the removal of H_2O (25–300 °C) and a steep loss associated with the removal of SO_3 (600–800 °C) from the surface. This feature is typical for sulfated zirconia [18,22]. The first loss is *ca.* 4 wt% and the second is *ca.* 39 wt%, meaning that the sulfur group (*i.e.*, SO_3) content was *ca.* 41 wt% in a dry state, *i.e.*, without adsorbed water. This value is quite higher than that found by Sun et al. [22] on the sulfated zirconia nanoparticles synthe-

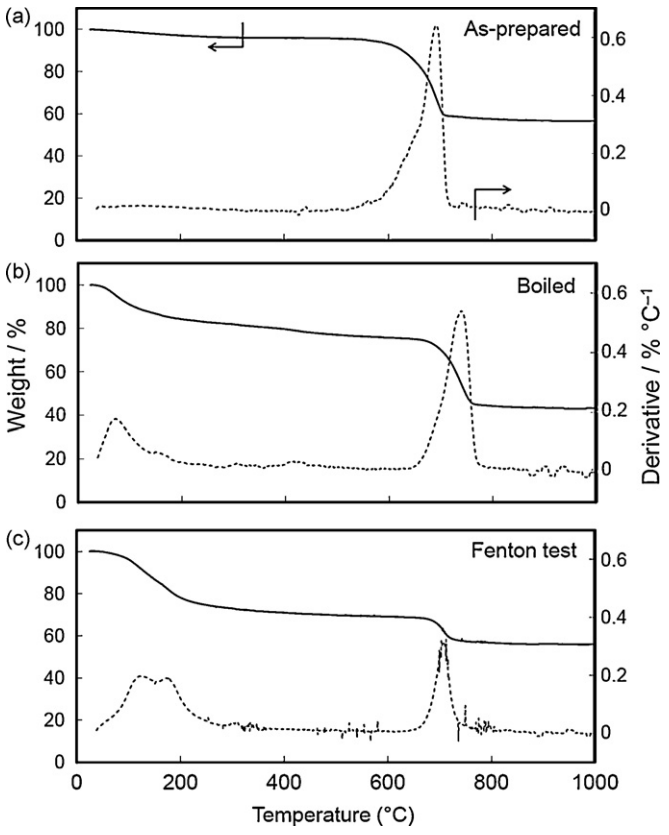

Fig. 5. TGA curves for the evaluation of chemical stability of sulfated zirconia. (a) As-prepared sample. (b) Sample after boiling treatment. (c) Sample after the Fenton test. Programming rate: 20 °C min^{-1} (25–300 °C) and 10 °C min^{-1} (300–1000 °C). Atmosphere: air ($60\,mL\,min^{-1}$).

sized by the same solvent-free method (7.7 wt%). This difference may be accounted for by considering the differences between ours and Sun's preparation method, *e.g.*, in the mixing procedure or in the air-flow rate.

Fig. 5b shows that, after boiling, the weight loss, attributed to the adsorbed H_2O removal, increased up to *ca.* 18 wt%, while the large weight loss for SO_3 groups appeared to be only slightly decreased to 33 wt%. The curve reveals another gradual weight loss of 6 wt% around 300–600 °C, *i.e.*, in a temperature range that is higher than that expected for the removal of surface adsorbed sulfuric acid [18]. This loss may be attributed to the transformation of the Brønsted acid sites to the Lewis acid sites [23], caused by the removal of H_2O molecules strongly bounded to the acid sites (Fig. 1). Quite likely, this transformation may induce a shift of the removal of SO_3 groups to higher temperature, *e.g.*, by 130 °C, than that related to as-prepared samples. The net weight loss for H_2O removal was determined to be 24 wt%. Consequently, the sulfur group content in the dry state was determined to be *ca.* 43 wt%, indicating that the sulfur groups were highly stable to hydrolysis (retention: ~100%). In addition, as previously reported [15], our samples are amorphous, which is a unique state for sulfated zirconia, typically reported as mixed monoclinic and tetragonal crystals [22]. This amorphous state was not affected by the boil treatment as determined by XRD (Fig. 2).

Fig. 5c shows the TGA result for the sample collected by filtration following the Fenton test. The treatment in the hydrogen peroxide solution led to an increase of the amount of H_2O up to *ca.* 31 wt%, and decreased the amount of SO_3 down to *ca.* 13 wt%. The sulfur group content in the dry state was determined to be *ca.* 19 wt% (retention: ~46%), thus, it was found that the surface sulfur groups were not completely stable to hydrogen peroxide. This degradation is probably due to the reaction of peroxide radicals with the strong acidic surface of the sulfated zirconia. In fact, during the Fenton test, vigorous bubble evolution was observed, probably originating from hydrogen peroxide catalytically decomposed on the sulfated zirconia surface. However, further study is certainly needed to fully clarify the reaction mechanism.

For sake of comparison, a typical Nafion 112 membrane was treated in the same Fenton reagent. As expected [24], the Nafion membrane exhibited weight losses in four temperature regions (Fig. 6a), *i.e.*: (i) a gradual loss up to ~100 °C attributed to the removal of bulk water, (ii) a slight loss around 200 °C attributed to strongly adsorbed water, (iii) a loss from 280 °C to 400 °C attributed to the sulfate group loss and (iv) a large loss above 400 °C attributed to the oxidative destruction of the perfluorinated matrix. Nafion is not too much damaged by the peroxide radicals under the experimental conditions (Fig. 6b), except for the shift of the onset temperature for the third loss toward lower temperature (from 280 °C to 250 °C). Compared with sulfated zirconia, Nafion seems to be more stable to peroxide radicals, probably because its molecules are less attacked than the sulfated zirconia nanoparticles.

3.3. Influence on Pt catalytic activity

It is known that the adsorption of anions, *e.g.*, sulfate ions, drastically reduces the activity of Pt catalysts. This important effect has been checked for the case of our sulfated zirconia using its dispersion with a concentration of 2.74 g L^{-1}, which is translated into a proton concentration of 8.2 mM using the acid content (3.0 mmol g^{-1} [15]) assuming that one proton dissociates from one sulfur group. The volume ratio of the sulfated zirconia to the dispersion is calculated as 0.17 vol% from the density of ZrO_2 (5.6 g cm^{-3}, 123 g mol^{-1}) and that of H_2SO_4 (1.84 g cm^{-3}, 178 g mol^{-1}) assuming that the sulfur groups became a form similar to H_2SO_4 in water (see Fig. 1). This low volume ratio clearly indicates that H_2O molecules played a role in the ionic conduction in this dispersion as is the case with typical aqueous electrolyte solutions. The ionic conductivity of this dispersion can be roughly calculated as 2.3 mS cm^{-1} from the data previously reported [15], 17 mS cm^{-1} at 20.4 g L^{-1}.

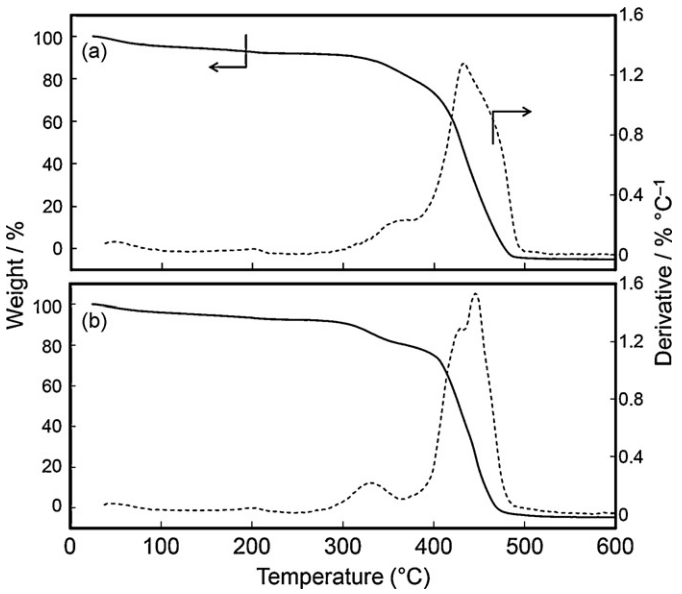

Fig. 6. TGA curves for the evaluation of chemical stability of a Nafion 112 membrane. (a) Pristine sample. (b) Sample after the Fenton test. Programming rate: 20 °C min^{-1} (25–200 °C) and 10 °C min^{-1} (200–600 °C). Atmosphere: air (60 mL min^{-1}).

The CV of a Pt electrode in a nitrogen-saturated sulfated-zirconia dispersion is reported in Fig. 7 in comparison with those obtained in H_2SO_4 solutions at different concentrations. Since we used RHE as the reference electrode to take care of different pH values, the CV traces reflect only the influence of anions and other adsorbable species. Fig. 7 demonstrates that the CV trend for sulfated-zirconia dispersion is similar to that obtained in H_2SO_4 solutions. The figure shows that faradaic currents attributable to the degradation of sulfated zirconia are not observed, meaning that our sulfated zirconia nanoparticles are electrochemically stable in the potential range of fuel cell reactions (*i.e.*, 0–1.2 V *vs.* RHE).

In the oxide region (*i.e.*, 0.7–1.2 V *vs.* RHE), the onset potential for the oxide formation and the oxide reduction peak potential around 0.8 V were shifted toward lower potentials, compared with those of H_2SO_4 solutions. However, this was not the case when comparing the CVs of the H_2SO_4 solutions at different concentrations. In general, such shift of the surface oxidation/reduction potentials is attributed to (i) adsorption of anions, which inhibits

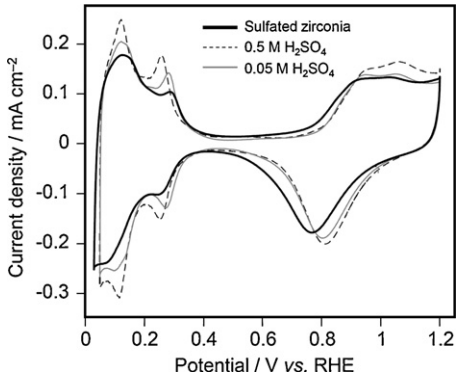

Fig. 7. CVs of a Pt electrode in different acid solutions. Bold solid line: sulfated-zirconia dispersion; dashed line: 0.5 M sulfuric acid solution; thin solid line: 0.05 M sulfuric acid solution. Scan rate: 50 mV s^{-1}.

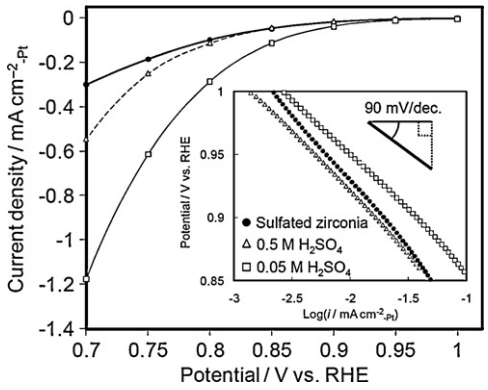

Fig. 8. Diffusion-corrected voltammograms of the oxygen reduction reaction on a Pt electrode in a sulfated-zirconia dispersion (circle plots), compared with those of 0.5 M sulfuric acid (triangle plots) and 0.05 M sulfuric acid (square plots). Inset: Tafel plots based on the original voltammograms at 500 rpm. Scan rate: 10 mV s^{-1} (negative scan). Electrochemical surface area obtained from a hydrogen adsorption charge of the CV in 0.5 M sulfuric acid was used as the area for calculating current density.

the surface oxidation/reduction reactions [25,26], or (ii) shift of *d*-band center, which increases the affinity of Pt surface to oxygen species. As for the former, the potentials in the case of H_2SO_4 were reported to shift toward higher than those of $HClO_4$ [27], which is known to negligibly adsorb onto Pt surface. As for the latter, when using transition metal oxides as catalyst supports [28], the surface oxidation/reduction reactions of Pt catalysts were reported to shift toward lower potentials. Thus, we may conclude that the shift is attributable to some unique properties of sulfated zirconia nanoparticles, probably associated with their modest adsorbability onto the Pt surface, or with strong interaction between sulfated zirconia and Pt surface. Since the ORR activity should be higher if the adsorption was negligible, the following ORR analysis suggests the possibility of the strong interaction caused by sulfated zirconia adsorption because the ORR activity in the sulfated-zirconia dispersion was lower than that in the 0.05 M H_2SO_4 solution. Though this hypothesis is partly confirmed by the influence of the nanoparticles on the ORR activity, further analyses are needed to conclude the mechanism.

In the hydrogen region (*i.e.*, 0–0.35 V *vs.* RHE), the CV peaks in the sulfated-zirconia dispersion are blunt compared with those of H_2SO_4 solutions. This is simply attributable to the ohmic drops caused by the larger ionic resistivity of the dispersion or maybe to the adsorption of the sulfated zirconia nanoparticles onto the Pt surface. In view of the fact that the peak height decreases by decreasing the H_2SO_4 concentration, we may assume that the decrease obtained for the sulfated zirconia is probably attributed to differences in the ohmic losses. This may be confirmed by our previous results which show that the resistivity of a sulfated-zirconia dispersion, whose concentration was 7 times higher than that used in this work, was twice that of 0.1 M H_2SO_4.

By using the sulfated-zirconia dispersion as a supporting electrolyte, the ORR and the HOR characteristics were evaluated. Fig. 8 compares the ORR performance of a Pt electrode in the dispersion saturated with oxygen with those in H_2SO_4 solutions. To eliminate the influence of oxygen diffusion, the hydrodynamic voltammograms (Fig. S1, supplementary information) were analyzed based on the Koutechý–Levich equation [29] (Figs. S2–S4, supplementary information), and the related diffusion-corrected voltammograms are shown in Fig. 8. These voltammograms indicate that, in the kinetically controlled region (potential range >0.85 V), the ORR current in the sulfated-zirconia dispersion was as large as that in a 0.5 M H_2SO_4 solution but smaller than that in a 0.05 M H_2SO_4 solution. Below 0.8 V, the current density in the dispersion decayed probably because of the larger ohmic drop. This consideration on the ohmic drop is discussed later.

Table 1
Pt electrode activity for the oxygen reduction reaction in sulfated-zirconia dispersion.

	Specific activity[a]/μA cm$^{-2}_{-Pt}$	Tafel slope[b]/mV dec.$^{-1}$
Sulfated-zirconia dispersion	17 ± 2	110
0.5 M H_2SO_4	15 ± 1	90
0.05 M H_2SO_4	32 ± 4	90

[a] Oxygen reduction current density at 0.9 V (*vs.* RHE) based on active surface area of the electrode obtained from the hydrogen desorption charge in 0.5 M H_2SO_4. These data were obtained at room temperature (~20 °C).
[b] The Tafel slopes were determined in the potential range of 0.95–1.0 V.

The specific activities, which are defined as the current densities based on electrochemically active surface areas, are summarized in Table 1. The activity in the dispersion is comparable to that in 0.5 M H_2SO_4 and half as large as that in 0.05 M H_2SO_4. The lower activity of the Pt catalyst in the higher concentration H_2SO_4 solution is attributed to the larger amount of surface adsorbate (*i.e.*, sulfate ions) blocking the active sites for the oxygen reduction. On the other hand, the lower activity of the Pt catalyst in the dispersion should be attributed to the adsorption of sulfated zirconia. This decrease in the activity is not only resulting from a site-blocking effect, but also from the high affinity to oxygen species, as indeed suggested from the CVs of Fig. 7. The hypothesis of the stabilization of the surface oxide is also supported by the difference in the Tafel slopes (see Table 1), that are *ca.* 110 mV dec.$^{-1}$ for the sulfated-zirconia dispersion and *ca.* 90 mV dec.$^{-1}$ for the sulfuric acid solutions. This difference suggests that the interaction between Pt catalyst and sulfated zirconia is quite strong, as a similar hypothesis reported when using transition metal oxides as catalyst supports [28]. Moreover, a decrease in Pt catalyst activity for the oxygen reduction reaction due to the stabilization of Pt–O bonds is widely known [30].

Fig. 9 compares the HOR performance of a Pt electrode in the sulfated-zirconia dispersion saturated with hydrogen with that in a 0.5 M H_2SO_4 solution. The limiting current densities match those obtained in 0.5 M H_2SO_4, this indicating that solubility and diffusivity of hydrogen are the same in both solutions. In the low overpotential region (0–0.1 V), linear behaviors with the same onset potentials were observed for both solutions, indicating that the behaviors are not dominated by the catalytic activities but rather by the ohmic losses of the solutions. To discuss more precisely, we analyzed the data using the Koutechý–Levich equation (Figs. S5 and S6, supplementary information), and obtained the

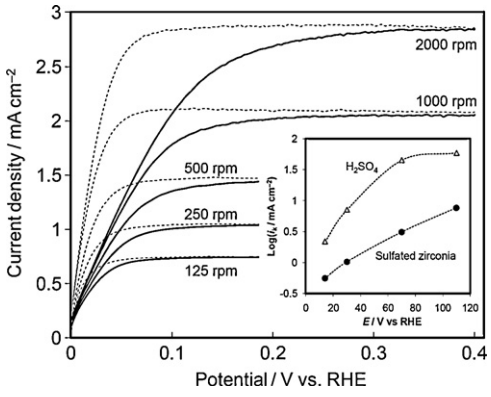

Fig. 9. Hydrodynamic voltammograms for the hydrogen oxidation reaction on a flat Pt electrode in a sulfated-zirconia dispersion (solid lines), compared with those of 0.5 M sulfuric acid (dashed lines). Scan rate: 10 mV s^{-1} (positive scan). The current densities were based on the geometrical surface area (the same electrode with a roughness factor of 3.2 was used). Inset: Tafel plots based on the kinetically controlled current densities.

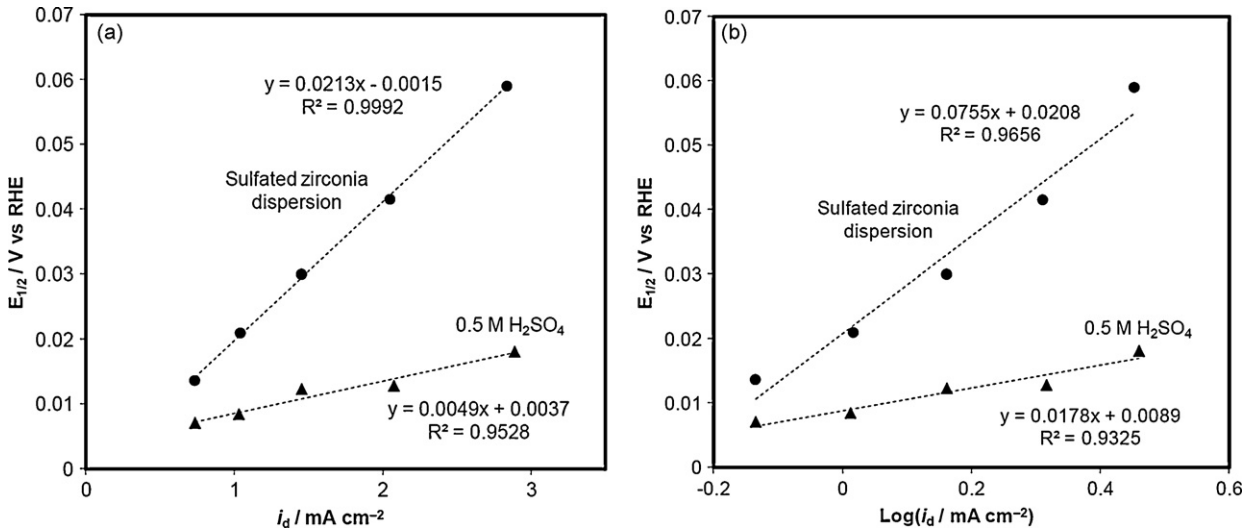

Fig. 10. Relation between the limiting diffusion current densities (i_d) and the half-wave potentials ($E_{1/2}$) for the hydrogen oxidation reaction on a Pt electrode in a hydrogen-saturated sulfated-zirconia dispersion or 0.5 M H_2SO_4 solution. (a) $E_{1/2}$ *vs.* i_d; (b) $E_{1/2}$ *vs.* $\log i_d$. The lines were obtained by the least-square fit.

Tafel plots based on the kinetically controlled current densities (inset, Fig. 9). This figure shows a possibility that the catalytic activity of the Pt electrode in the sulfated-zirconia dispersion (0.56 mA cm^{-2} at 14 mV) was lower than that in the H_2SO_4 solution (2.2 mA cm^{-2} at 14 mV). However, this is probably more complicated situation, because the Tafel plots show non-linear relations, which mean that the reaction was not kinetically controlled.

The ohmic resistance of the solution is considered to decrease the activation overpotential, resulting in the non-linear behavior of the Tafel plots. To elucidate the influence of the ohmic drop, we plotted the half-wave potentials, $E_{1/2}$, against the limiting diffusion current densities, i_d, in Fig. 10, because they have the following relation (details are shown in the supplementary information file):

$$E_{1/2} = b \cdot \log\left(\frac{i_d}{i_0}\right) + \frac{R_{loss}}{2} i_d \quad (1)$$

$$b = -\frac{RT}{\alpha n F \cdot \log e} \quad (2)$$

where i_0 is the exchange current density, α the transfer coefficient, n the number of charge transfer for the rate determining step, F the Faraday constant, R_{loss} the ohmic resistance, R the molar gas constant, and T is the absolute temperature. Since a clear linear relation was obtained for the sulfated zirconia solution, the half-wave potentials are considered to be limited by the ohmic loss. This consideration is reasonable because the HOR on a Pt electrode is known to be considerably fast, *i.e.*, quite large i_0. The ohmic resistance was estimated as at most 42.6 Ω cm^2 from the gradient of the fitting line, and it causes an ohmic loss of 42.6 mV at 1 mA cm^{-2}. Thus, we found that the activity difference obtained from Fig. 9 was attributed mainly to this ohmic loss, that is, sulfated zirconia did not cause an obvious decrease in the catalytic activity of Pt for the HOR. As for the HOR in the 0.5 M H_2SO_4 solution, since the correlation coefficients of Fig. 10a and b were similar, the reaction was considered to be dominated by both the ohmic loss and the kinetics.

4. Conclusion

In this paper, we show that sulfated zirconia is a promising proton conductor for polymer electrolyte fuel cells since it benefits by high conductivity, electrochemical stability, chemical stability to hydrolysis, relatively low influence on catalyst activity and ease of synthesis. These features are attractive and suggest that other superacid oxides (*e.g.*, sulfated titania) may also be promising materials as new proton conductors in replacement of common organic proton conductors. We believe that the results here reported provide a valid basis to reach the final goal of making these superacid oxides of practical value as proton conductors for fuel cells.

Acknowledgements

This work was partly supported by the Grant-in-Aid for Specially Promoted Research "Establishment of Electrochemical Device Engineering" and by the Global COE program "Practical Chemical Wisdom" from the Ministry of Education, Culture, Sports, Science and Technology, Japan.

Appendix A. Supplementary data

Supplementary data associated with this article can be found, in the online version, at doi:10.1016/j.jpowsour.2010.01.053.

References

[1] S. Licoccia, E. Traversa, J. Power Sources 159 (2006) 12–20.
[2] V. Neburchilov, J. Martin, H. Wang, J. Zhang, J. Power Sources 169 (2007) 221–238.
[3] K. Miyatake, Y. Chikashige, E. Higuchi, M. Watanabe, J. Am. Chem. Soc. 129 (2007) 3879–3887.
[4] S. Hara, M. Miyayama, Solid State Ionics 168 (2004) 111–116.
[5] T. Sancho, J. Lemus, M. Urbiztondo, J. Soler, M.P. Pina, Micropor. Mesopor. Mater. 115 (2008) 206–213.
[6] N. Giordano, A.S. Arico, S. Hocevar, P. Staiti, P.L. Antonucci, V. Antonucci, Electrochim. Acta 38 (1993) 1733–1741.
[7] N. Giordano, P. Staiti, S. Hocevar, A.S. Arico, Electrochim. Acta 41 (1996) 397–403.
[8] S. Hara, S. Takano, M. Miyayama, J. Phys. Chem. B 108 (2004) 5634–5639.
[9] D. Sarkar, D. Mohapatra, S. Ray, S. Bhattacharyya, S. Adak, N. Mitra, Ceram. Int. 33 (2007) 1275–1282.
[10] M.A. Navarra, C. Abbati, B. Scrosati, J. Power Sources 183 (2008) 109–113.
[11] M.A. Navarra, F. Croce, B. Scrosati, J. Mater. Chem. 17 (2007) 3210–3215.
[12] P. Choi, N.H. Jalani, R. Datta, J. Electrochem. Soc. 152 (2005) A1548–A1554.
[13] S.Z. Ren, G.Q. Sun, C.N. Li, S.Q. Song, Q. Xin, X.F. Yang, J. Power Sources 157 (2006) 724–726.
[14] Y. Zhang, H.M. Zhang, X.B. Zhu, C. Bi, J. Phys. Chem. B 111 (2007) 6391–6399.
[15] S. Tominaka, N. Akiyama, F. Croce, T. Momma, B. Scrosati, T. Osaka, J. Power Sources 185 (2008) 656–663.
[16] M.G. Cutrufello, U. Diebold, R.D. Gonzalez, Catal. Lett. 101 (2005) 5–13.
[17] D. Fărcaşiu, J.Q. Li, S. Cameron, Appl. Catal. A: Gen. 154 (1997) 173–184.
[18] M. Hino, M. Kurashige, H. Matsuhashi, K. Arata, Thermochim. Acta 441 (2006) 35–41.
[19] V. Parvulescu, S. Coman, P. Grange, V.I. Parvelescu, Appl. Catal. A: Gen. 176 (1999) 27–43.
[20] K. Arata, M. Hino, Mater. Chem. Phys. 26 (1990) 213–237.

[21] C. Morterra, G. Cerrato, S. Ardizzone, C.L. Bianchi, M. Signoretto, F. Pinna, Phys. Chem. Chem. Phys. 4 (2002) 3136–3145.
[22] Y.Y. Sun, S.Q. Ma, Y.C. Du, L. Yuan, S.C. Wang, J. Yang, F. Deng, F.S. Xiao, J. Phys. Chem. B 109 (2005) 2567–2572.
[23] M.K. Mishra, B. Tyagi, R.V. Jasra, Ind. Eng. Chem. Res. 42 (2003) 5727–5736.
[24] S.R. Samms, S. Wasmus, R.F. Savinell, J. Electrochem. Soc. 143 (1996) 1498–1504.
[25] S. Tominaka, C.-W. Wu, K. Kuroda, T. Osaka, J. Power Sources 195 (2010) 2236–2240.
[26] J.X. Wang, N.M. Markovic, R.R. Adzic, J. Phys. Chem. B 108 (2004) 4127–4133.
[27] J. Sobkowski, K. Franaszczuk, K. Dobrowolska, J. Electroanal. Chem. 330 (1992) 529–540.
[28] S.G. Neophytides, K. Murase, S. Zafeiratos, G. Papakonstantinou, F.E. Paloukis, N.V. Krstajic, M.M. Jaksic, J. Phys. Chem. B 110 (2006) 3030–3042.
[29] A.J. Bard, L.R. Faulkner, Electrochemical Methods: Fundamentals and Applications, 2nd ed., John Wiley & Sons, Inc., New York, 2001, pp. 340–344.
[30] J. Greeley, I.E.L. Stephens, A.S. Bondarenko, T.P. Johansson, H.A. Hansen, T.F. Jaramillo, J. Rossmeisl, I. Chorkendorff, J.K. Norskov, Nat. Chem. 1 (2009) 552–556.
[31] V. Bolis, G. Magnacca, G. Cerrato, C. Morterra, Langmuir 13 (1997) 888–894.